Commun Nonlinear Sci Numer Simulat 15 (2010) 2565–2574

Contents lists available at ScienceDirect

Commun Nonlinear Sci Numer Simulat

journal homepage: www.elsevier.com/locate/cnsns

Design constraints for third-order PLL nodes in master-slave clock distribution networks

A.M. Bueno, A.G. Rigon, A.A. Ferreira, José R.C. Piqueira *

Departamento de Engenharia de Telecomunicacoes e Controle Escola Politecnica-Universidade de São Paulo Sao Paulo - Brazil

ARTICLE INFO

Article history:
Received 17 July 2009
Accepted 29 September 2009
Available online 9 October 2009

Keywords:
Phase-locked loop
Second-order filter
Synchronization
Stability

ABSTRACT

Clock signal distribution in telecommunication commercial systems usually adopts a master-slave architecture, with a precise time basis generator as a master and phase-locked loops (PLLs) as slaves. In the majority of the networks, second-order PLLs are adopted due to their simplicity and stability. Nevertheless, in some applications better transient responses are necessary and, consequently, greater order PLLs need to be used, in spite of the possibility of bifurcations and chaotic attractors. Here a master-slave network with third-order PLLs is analyzed and conditions for the stability of the synchronous state are derived, providing design constraints for the node parameters, in order to guarantee stability and reachability of the synchronous state for the whole network. Numerical simulations are carried out in order to confirm the analytical results.

1. Introduction

Synchronization networks assure the correct temporal order of information processing in communication systems, computation and control [1,2]. Many commercial systems adopt the One-way Master-slave (OWMS) synchronization strategy due to its reliable behavior, construction facility and low cost [1–3].

In this kind of arrangement, the master node (node 1) generates a precise clock signal. This signal is sent to the first slave node (node 2) which extracts the time basis and sends it to the following node. This process is repeated up to the last node (node N) [2].

Each slave node is built with a PLL that is a closed loop composed of a phase-detector (PD), a low-pass filter (F) and a voltage controlled oscillator (VCO). The PLLs are described by a differential equation of order $P + 1$, considering that the order of the filter is P [2,4].

Therefore, the PLL plays an important role in the performance of the whole distribution network as the individual node errors can be accumulated and transmitted to the sequential nodes [5].

Stable operation with a second-order PLL is simple and reliable because its linearized model presents open loop transfer function with two poles and one zero [6]. A pole creates a phase shift of $-90°$ at the higher frequencies, and the zero creates a phase shift of $+90°$. If the poles and zeros are properly located, the overall phase shift never comes close to $-180°$.

* Corresponding author. Address: Escola Politécnica da Universidade de São Paulo, Avenida Prof. Luciano Gualberto, travessa 3, n. 158, 05508-900, São Paulo, SP, Brazil. Tel.: +55 11 30915647; fax: +55 11 30915718.
E-mail address: piqueira@lac.usp.br (J.R.C. Piqueira).

1007-5704/$ - see front matter © 2009 Elsevier B.V. All rights reserved.
doi:10.1016/j.cnsns.2009.09.039

In spite of second-order PLL qualities, there are some situations in which their performance is spoiled by double-frequency distortions due to the nonlinear operation of the PD [7,8]. This effect appears as an oscillation around the synchronous state in the slave nodes of a OWMS clock distribution system [9,10]. Additionally, the sensitivity to drifts in the master clock limits the network quality figures [11]. Another important point is that the frequency jumps inherent to the second-order loop usually cannot be accepted and additional filtering is necessary [12].

To minimize these double-frequency oscillations, drifts and jumps, third-order PLLs are used to improve the reachability of the synchronous state. Most actual PLLs contain additional poles at higher frequency deliberately inserted to suppress higher-frequency disturbances emanating from the phase detector [6] (p. 25).

In spite of the relevance of the problem, it does not appear a lot in the literature [12]. An important paper about third-order PLLs is [13], developing a model to be applied to complex systems that can be composed of interconnected PLLs is being used as a good reference.

Another seminal work about higher-order PLLs is [14] with an extensive analysis of stability and reachability of the synchronous state in the single node case, for practical PLL integrated circuits and it is shown that they can provide lesser acquisition times [15]. On the other hand, bifurcations appear implying that filter parameters need to be chosen in a very accurate way [16–18].

Here, a model for an OWMS clock distribution system is developed, considering third-order PLLs, equipped with second-order filters, as implemented in the most commercial components [19]. By using this model, a condition for stability of the synchronous state relating the filter parameters is derived, being a necessary condition for the lock-in range of the network. Numerical simulations are carried out in order to confirm the analytical results and to provide a better understanding of the network behavior.

In Section 2, an analytical model for one-way master-slave networks, following the work presented in [18] and extending it for third-order nodes. In Section 3, conditions for the synchronous stability of the whole network modeled in Section 2 are derived.

Results of Section 3 are the core of this contribution, with Eqs. (27) and (28) providing a design criterion for the node parameters, allowing how to choose them, in order to guarantee the stability of the synchronous state of the whole network, complementing the results presented in [15–17] for isolated nodes.

Section 4 presents numerical simulations confirming the analytical reasoning presented in Section 3. Section 5 touches the reachability problem showing that, under conditions of Eqs. (27) and (28), the synchronous state in always reachable, even if some cycle-slip occurs. A summary of conclusions is presented in Section 6.

2. One-Way Master-Slave architecture model

In this section, an analytical model for the OWMS architecture is developed, based on the model of a single PLL. The master node (1) is considered to be a precise time basis generator and the slave nodes (2 to N) are third-order PLLs [2,6].

In each slave node, the VCO local phase, θ_o, is controlled by the input phase, θ_i, that comes from the master for node 2 and from node $n-1$ for each node $n>2$.

The master clock (node 1) is supposed to be a stable and accurate oscillator given by:

$$v_o^{(1)}(t) = v_o^{(1)} \cos(\omega_M t + \theta_o^{(1)}(t)), \tag{1}$$

where v_o is the amplitude of the master node output, ω_M is the free-running angular frequency, and $\theta_o^{(1)}(t)$ is the reference phase signal.

At a slave n-node ($n \geqslant 2$), the input signal $v_i^{(n)}(t)$ and the VCO output $v_o^{(n)}(t)$ are supposed to have the same free running frequency ω_M and their expressions, as each node generates a phase shift of $(n-1)\frac{\pi}{2}$ [2,3,6,19], are given by:

$$v_i^{(n)}(t) = v_o^{(n-1)} \sin\left(\omega_M t + \theta_o^{(n-1)}(t) + (n-1)\frac{\pi}{2}\right); \tag{2}$$

$$v_o^{(n)}(t) = v_o^{(n)} \cos\left(\omega_M t + \theta_o^{(n)}(t) + (n-1)\frac{\pi}{2}\right), \tag{3}$$

with v_o representing the amplitude of the signals.

The filter is considered to be stable linear low-pass, with transfer function $F(s)$, as used in the main commercial integrated PLL [19], given by:

$$F^{(n)}(s) = \frac{\alpha_1^{(n)} s + \alpha_0^{(n)}}{\beta_2^{(n)} s^2 + \beta_1^{(n)} s + \beta_0^{(n)}}. \tag{4}$$

Defining local phase error:

$$\varphi^{(n)}(t) \equiv \theta_0^{(n-1)}(t) - \theta_o^{(n)}(t), \tag{5}$$

the output of the PD is:

$$v_d^{(n)}(t) = v_o^{(n-1)}(t)\, v_o^{(n)}(t). \tag{6}$$

After replacing Eqs. (2) and (3) into (6) and doing some algebra, the output of the PD is:

$$v_d^{(n)}(t) = \frac{G^{(n)}}{k_o^{(n)}} \sin(\varphi^{(n)}(t)). \tag{7}$$

The global gain G of the node is given by:

$$G^{(n)} = \frac{k_m^{(n)} k_o^{(n)} v_o^{(n-1)} v_o^{(n)}}{2}, \tag{8}$$

where k_m is the PD gain and k_o, the VCO gain.

In Eq. (7), the double-frequency term was neglected because it is supposed to be filtered [6,9,10,19].

The output phase $\theta_o^{(n)}$ of the VCO is controlled according to the relation:

$$\dot{\theta}_o^{(n)}(t) = k_o^{(n)} v_c^{(n)}(t), \tag{9}$$

where $v_c^{(n)}$ is given by:

$$v_c^{(n)}(t) = \int_0^t f^{(n)}(t-\tau) v_d^{(n)}(\tau)\, d\tau, \tag{10}$$

resulting, after replacing (10) into (9):

$$\dot{\theta}_o^{(n)}(t) = k_o^{(n)} \int_0^t f^{(n)}(t-\tau) v_d^{(n)}(\tau)\, d\tau. \tag{11}$$

Considering the former relations and applying the convolution theorem [20] in Eq. (11), the dynamics of the slave nodes is according to:

$$\begin{aligned} &\beta_2^{(n)} \dddot{\varphi}^{(n)}(t) + \beta_1^{(n)} \ddot{\varphi}^{(n)}(t) + \beta_0^{(n)} \dot{\varphi}^{(n)}(t) + \alpha_1^{(n)} G^{(n)} \dot{\varphi}^{(n)}(t) \cos(\varphi^{(n)}(t)) + \alpha_0^{(n)} G^{(n)} \sin\left(\varphi^{(n)}(t)\right) \\ &\quad = \beta_2^{(n)} \dddot{\theta}_o^{(n-1)}(t) + \beta_1^{(n)} \ddot{\theta}_o^{(n-1)}(t) + \beta_0^{(n)} \dot{\theta}_o^{(n-1)}(t), \end{aligned} \tag{12}$$

for $n = 2, \ldots, N$.

Eq. (12) relates the phase error $\varphi^{(n)}(t)$ to the phase of the input signal $\theta_o^{(n-1)}(t)$, for any node $n \geqslant 2$ of the network and can be transformed in state equations defining:

$$x_1^{(m)} = \varphi^{(n)}(t), \tag{13}$$

$$x_2^{(m)} = \dot{\varphi}^{(n)}(t), \tag{14}$$

$$x_3^{(m)} = \ddot{\varphi}^{(n)}(t), \tag{15}$$

therefore,

$$\begin{aligned} \dot{x}_1^{(m)} &= x_2^{(m)} \\ \dot{x}_2^{(m)} &= x_3^{(m)} \\ \dot{x}_3^{(m)} &= -\mu_{\beta 1}^{(m)} x_3^{(m)} - \mu_{\beta 0}^{(m)} x_2^{(m)} - \mu_{\alpha 1}^{(m)} x_2^{(m)} \cos\left(x_1^{(m)}\right) \\ &\quad - \mu_{\alpha 0}^{(m)} \sin(x_1^{(m)}) \end{aligned} \tag{16}$$

for $m = n - 1$, and

$$\mu_{\alpha 0}^{(m)} = \frac{\alpha_0^{(n)} G^{(n)}}{\beta_2^{(n)}}, \tag{17}$$

$$\mu_{\alpha 1}^{(m)} = \frac{\alpha_1^{(n)} G^{(n)}}{\beta_2^{(n)}}, \tag{18}$$

$$\mu_{\beta 0}^{(m)} = \frac{\beta_0^{(n)}}{\beta_2^{(n)}}, \tag{19}$$

$$\mu_{\beta 1}^{(m)} = \frac{\beta_1^{(n)}}{\beta_2^{(n)}}. \tag{20}$$

Expression (16) describes the dynamics of the phase adjustments for a slave n-node in a OWMS network, depending on the parameters of the filter and on the global gain of the node.

Defining that the network reaches a synchronous state when all local phase errors, $\varphi^{(n)}(t)$, reach constant values, these synchronous states correspond to the equilibrium states of Eq. (16). In the next section, synchronous states and conditions for their stability are presented.

3. OWMS network synchronous state stability

In this section, the stability of the synchronous state is studied, i.e., if the reachable synchronous state is robust under small perturbations. The analysis is performed considering the first term in the Taylor's series around the equilibrium points, which are hyperbolic [21].

The equilibrium points of the state equations in (16) are:

$$\mathbf{x}^{*(m)} = [\,k\pi \quad 0 \quad 0\,]^T \tag{21}$$

where $k = 0, \pm1, \pm2, \ldots$, and $m = 1, 2, \ldots, N-1$, then:

$$\mathbf{x}^{*} = \left[\,\mathbf{x}^{*(1)T} \quad \mathbf{x}^{*(2)T} \quad \ldots \quad \mathbf{x}^{*(N-1)T}\,\right]^T. \tag{22}$$

The equilibrium points for $k = 1, 3, 5, \ldots$ are unstable for any parameter combination [16,17,15].

Consequently, the reachable synchronous states correspond to even values of k and their stability conditions can be studied by determining the eigenvalues of the Jacobian matrix of Eq. (23), $\mathbf{A}$, calculated at the equilibrium point $\mathbf{x}^{*}$, with $k = 0$. Therefore,

$$\mathbf{A} = \begin{bmatrix} \mathbf{A}^{(1)} & \mathbf{0} & \cdots & \mathbf{0} \\ \mathbf{0} & \mathbf{A}^{(2)} & \cdots & \mathbf{0} \\ \vdots & \vdots & \ddots & \vdots \\ \mathbf{0} & \mathbf{0} & \ldots & \mathbf{A}^{(N-1)} \end{bmatrix}, \tag{23}$$

where

$$\mathbf{A}^{(m)} = \begin{bmatrix} 0 & 1 & 0 \\ 0 & 0 & 1 \\ -\mu_{\alpha 0}^{(m)} & -\left(\mu_{\beta 0}^{(m)} + \mu_{\alpha 1}^{(m)}\right) & -\mu_{\beta 1}^{(m)} \end{bmatrix}. \tag{24}$$

The characteristic polynomial of the matrix $\mathbf{A}$ is the product:

$$P(\lambda) = \prod_{m=1}^{N-1} P^{(m)}(\lambda), \tag{25}$$

with

$$P^{(m)}(\lambda) = \lambda^3 + \mu_{\beta 1}^{(m)}\lambda^2 + \left(\mu_{\beta 0}^{(m)} + \mu_{\alpha 1}^{(m)}\right)\lambda + \mu_{\alpha 0}^{(m)}. \tag{26}$$

Eqs. (25) and (26) imply that the reachable synchronous states of the OWMS network are locally asymptotically stable if, and only if, the synchronous states of each node are locally asymptotically stable.

The signals of the real parts of the roots of Eqs. (25) and (26) can be determined applying the Routh–Hurwitz criterion [22] as follows:

$$\begin{array}{c|cc} \lambda^3 & 1 & \mu_{\beta 0}^{(m)} + \mu_{\alpha 1}^{(m)} \\ \lambda^2 & \mu_{\beta 1}^{(m)} & \mu_{\alpha 0}^{(m)} \\ \lambda^1 & \dfrac{\mu_{\beta 1}^{(m)}\left(\mu_{\beta 0}^{(m)} + \mu_{\alpha 1}^{(m)}\right) - \mu_{\alpha 0}^{(m)}}{\mu_{\beta 1}^{(m)}} & \\ \lambda^0 & \mu_{\alpha 0}^{(m)} & \end{array}$$

As all the coefficients of the characteristic equation are positive real numbers in possible physical situations, all the roots have negative real parts if:

$$\mu_{\beta 1}^{(m)}\left(\mu_{\beta 0}^{(m)} + \mu_{\alpha 1}^{(m)}\right) > \mu_{\alpha 0}^{(m)}. \tag{27}$$

Replacing Eqs. (17)–(20) into (27) and doing some algebra:

$$G^{(n)} < \frac{\beta_0^{(n)}\beta_1^{(n)}}{\alpha_0^{(n)}\beta_2^{(n)} - \alpha_1^{(n)}\beta_1^{(n)}}, \tag{28}$$

for $n = 2, 3, \ldots, N$, giving a superior limit to each node gain $G^{(n)}$, depending on the filter transfer function coefficients. Consequently, if the inequality in expression (28) is satisfied, the network reaches an asymptotically stable synchronous state.

The conclusion concerning the loop gain is different if a particular case of the loop filter (Eq. (4)) is used. Considering, for instance, $\alpha_0^{(n)} = 1,\ \beta_0^{(n)} = 0$ and $\beta_1^{(n)} = 1$, the filter transfer function in Eq. (4) is then given by:

$$F^{(n)}(s) = \frac{\alpha_1^{(n)}s + 1}{s(\beta_2^{(n)}s + 1)}, \tag{29}$$

combining a first order lead-lag with a pure integration.

Replacing the coefficients of Eq. (29) into the coefficients (Eqs. (17)–(20)) of the state space model (Eq. (16)), result:

$$\mu_{\alpha 0}^{(m)} = \frac{G^{(n)}}{\beta_2^{(n)}}, \tag{30}$$

$$\mu_{\alpha 1}^{(m)} = \frac{\alpha_1^{(n)}G^{(n)}}{\beta_2^{(n)}}, \tag{31}$$

$$\mu_{\beta 0}^{(m)} = 0, \tag{32}$$

$$\mu_{\beta 1}^{(m)} = \frac{1}{\beta_2^{(n)}}. \tag{33}$$

By following the previous steps and replacing Eqs. (30)–(33) into (27), the roots of the characteristic polynomial (Eq. (26)) have negative real parts if:

$$\alpha_1^{(n)} > \beta_2^{(n)}. \tag{34}$$

Consequently, if the filter of the loop combines a fist order lead-lag with a pure integration and expression (34) is satisfied, the network reaches an asymptotically stable synchronous state. In this case, however, there is no superior limit for the loop gain $G^{(n)}$.

4. Numerical simulations

In order to confirm the analytical results, OWMS networks with a master and four slaves are simulated with built in Simulink blocks, using the "Ode45 Dormand-Prince" integration method [23]. The central angular frequency is normalized to $\omega_M = 1$ rad/s.

Three different filters are considered:

$$F_1^{(n)}(s) = \frac{s + 2}{s^2 + s + 1}, \tag{35}$$

$$F_2^{(n)}(s) = \frac{1.5s + 1}{s(s + 1)}, \tag{36}$$

and

$$F_3^{(n)}(s) = \frac{0.9s + 1}{s(s + 1)}. \tag{37}$$

According to expression (28), the network with filter F_1 (Eq. (35)) reaches an asymptotically stable synchronous state if $G^{(n)} < 1$. The results for simulations with $G^{(n)} = 0.5$ and $G^{(n)} = 2$ are shown in Figs. 1 and 2, respectively. As expected, all the slave nodes reach the synchronous state for $G^{(n)} = 0.5$ and, for $G^{(n)} = 2$, the synchronous states are unreachable for any node.

Results considering the filters described by (36) and (37) (with $G^{(n)} = 0.5$ in both cases) are shown in Figs. 3 and 4, respectively.

In Fig. 3, the network nodes reach synchronous states, as expected, since the parameters of F_2 satisfy inequality (34). For F_3, inequality (34) is not satisfied, and the synchronous states are unreachable in the state space.

For the same loop gain ($G^{(n)} = 0.5$) and cut-off frequency of the filters ($\omega_c = 2$ rad/s), the network presents better transient response with filter F_1 than with filter F_2 (see Figs. 1 and 3).

However, as shown in the last section, using filters combining pure integration with a first order lead-lag imposes no upper limit on the loop gain. This can be used to improve the transient response.

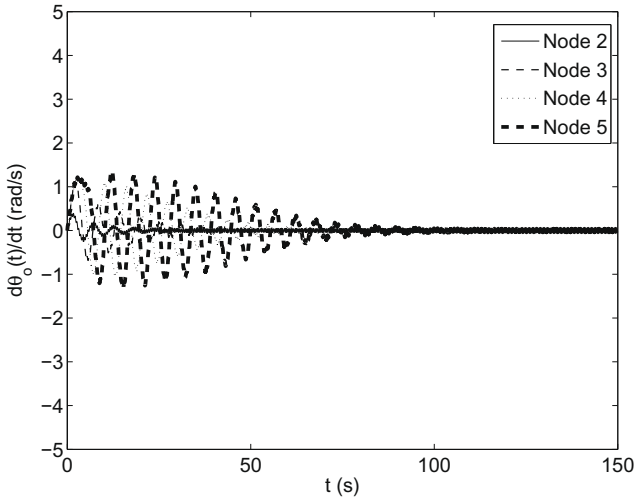

Fig. 1. OWMS network simulation with F_1 and $G^{(n)} = 0.5$.

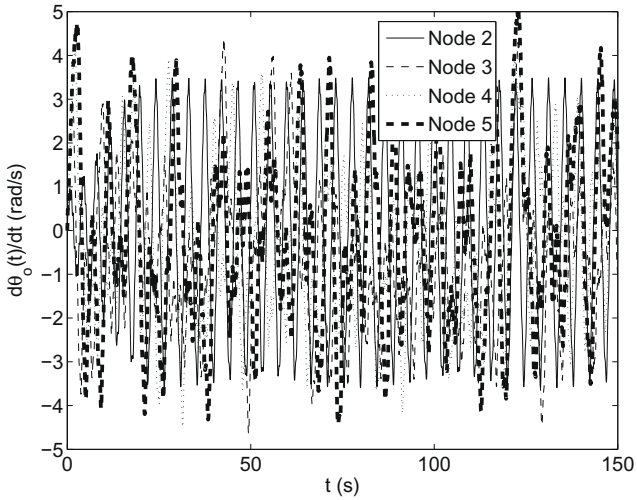

Fig. 2. OWMS network simulation with F_1 and $G^{(n)} = 2$.

5. Reachability of the synchronous states

In Section 3, the problem of determining the local stability conditions of the synchronous state for OWMS networks with third order PLLs was addressed. However, the search for global stability conditions is also important, since they are related to the reachability of the synchronous states [24].

The study of the global stability conditions requires the explicit knowledge of a Lyapunov function [25,26]. Since there is no straightforward method, the search for a Lyapunov function is frequently cumbersome.

A simpler goal is to observe how the trajectories behave in a bounded region of the state space, i.e., all the observed trajectories having their origins in a fixed (thus arbitrarily large) bounded region. Here, this problem is approached numerically.

Since the equilibrium points of Eq. (16) are repeated periodically in the state space, with the same structural characteristics [15–17], the region in the state space is chosen so as to include the origin. Then, the region is defined by the set:

$$R^{(m)} = \left\{ \left[x_1^{(m)} x_2^{(m)} x_3^{(m)} \right]^T \mid -3\pi < x_1^{(m)} < 3\pi, -3\pi < x_2^{(m)} < 3\pi, -3\pi < x_3^{(m)} < 3\pi \right\}, \tag{38}$$

including three stable ($[-2\pi\ 0\ 0]^T$, $[0\ 0\ 0]^T$, $[2\pi\ 0\ 0]^T$) and two unstable ($[-\pi\ 0\ 0]^T$, $[\pi\ 0\ 0]^T$) equilibrium points.

In Figs. 5 and 6, the state space plots of a single node, considering filters F_1 (Eq. (35)) and F_2 (Eq. (36)), respectively, are shown. In both cases, the trajectories represented by the thicker black lines start near a stable equilibrium point and, over time, the trajectories reach the synchronous states.

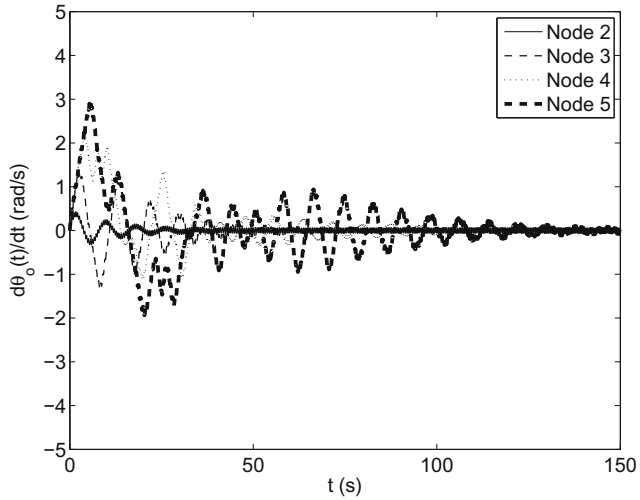

Fig. 3. OWMS network simulation with $F_2(\alpha_1^{(n)} = 1.5, \beta_2^{(n)} = 1)$.

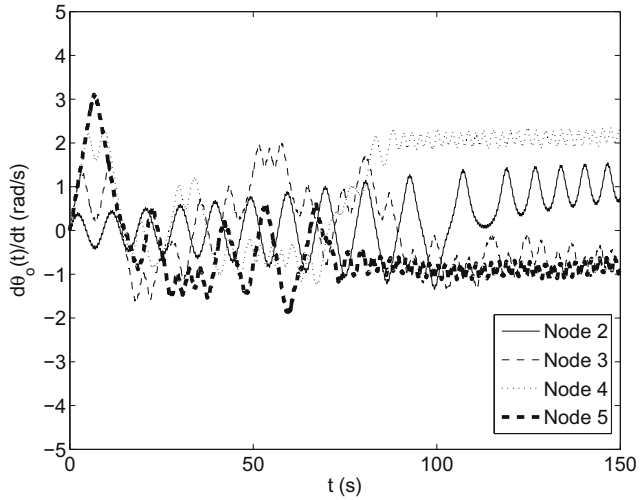

Fig. 4. OWMS network simulation with $F_3\left(\alpha_1^{(n)} = 0.9, \beta_2^{(n)} = 1\right)$.

Observing trajectories T_1, T_2 and T_3 in Fig. 5, it can be seen that, although all of them start within R, T_2 leaves R and does not return (see Fig. 5(a)–(c)). The same occurs with trajectory T_1 in Figs. 6(a)–(c).

However, it can be observed in trajectories T_2 (Fig. 5(d)) and T_1 (Fig. 6(d)) that the amplitude of the state variables x_2 and x_3 decay with time. Then, the tajectories that leave R also reach the synchronous state, i.e., a stable equilibrium point; but, in this case, outside R.

Only the two behaviors described above were observed in all the numerical simulations, which suggests that all the trajectories within R reach a synchronous state. Moreover, since the equilibrium points of Eq. (16) are repeated periodically in the state space, with the same structural characteristics, it also suggests that defining R so as to include all the possible values of x_1 would not affect the conclusions.

6. Conclusion

In an OWMS clock distribution system with third order PLLs, if the filter has the transfer function given by Eq. (4), then expression (28) states that there is a superior limit to the loop gain. On the other hand, if the loop filter combines a first order lead-lag with a pure integration, as in Eq. (29), the loop gain has no superior limit. Moreover, expressions (28) and (34) determine the conditions for the existence of synchronous states in OWMS networks. Consequently, designing conditions for this kind of clock distribution networks are well established, allowing how to choose node parameters, in order to have stable and reachable synchronous state for the whole system.

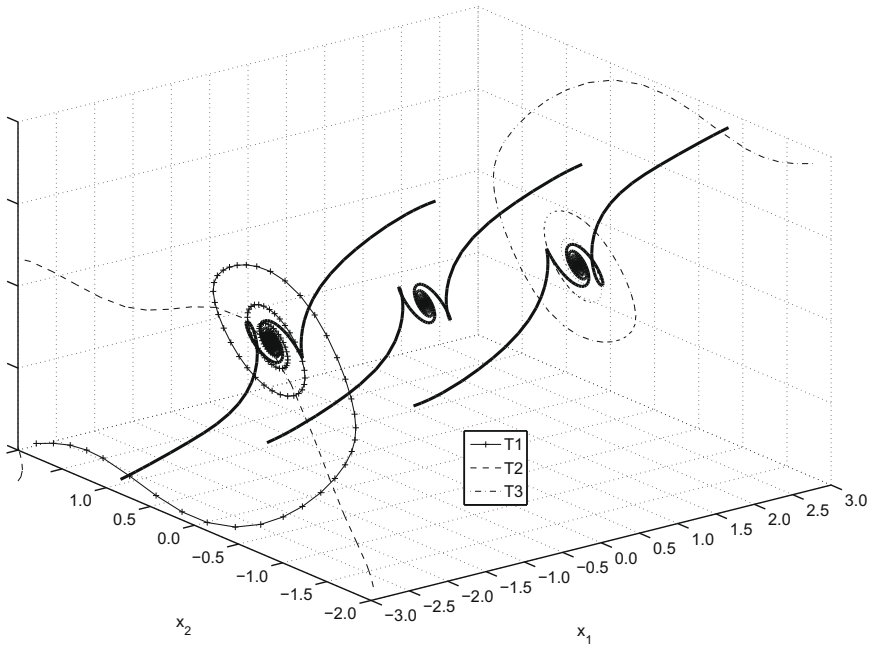

(a) 3D view.

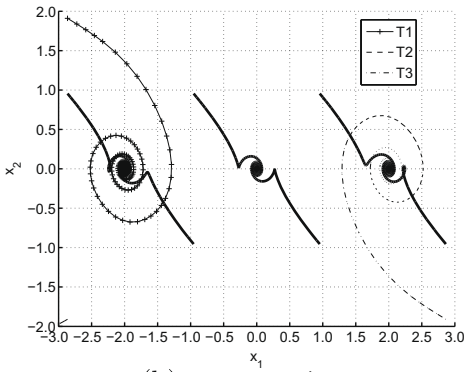

(b) $x_1 \times x_2$ view.

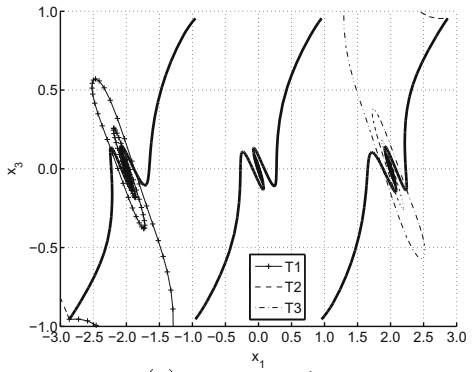

(c) $x_1 \times x_3$ view.

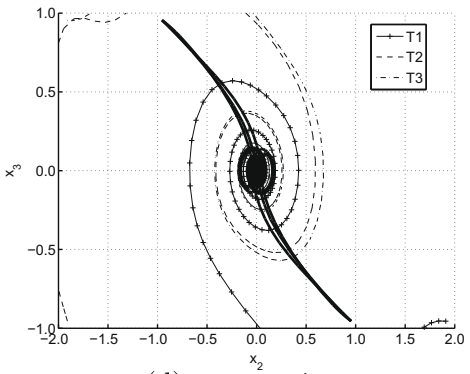

(d) $x_2 \times x_3$view.

Fig. 5. State space plot considering filter F_1, in units of π.

The numerical simulations presented in Section 5 suggest that all the trajectories within a bounded region R reach a synchronous state, which give insights on the study of the synchronous state reachability.

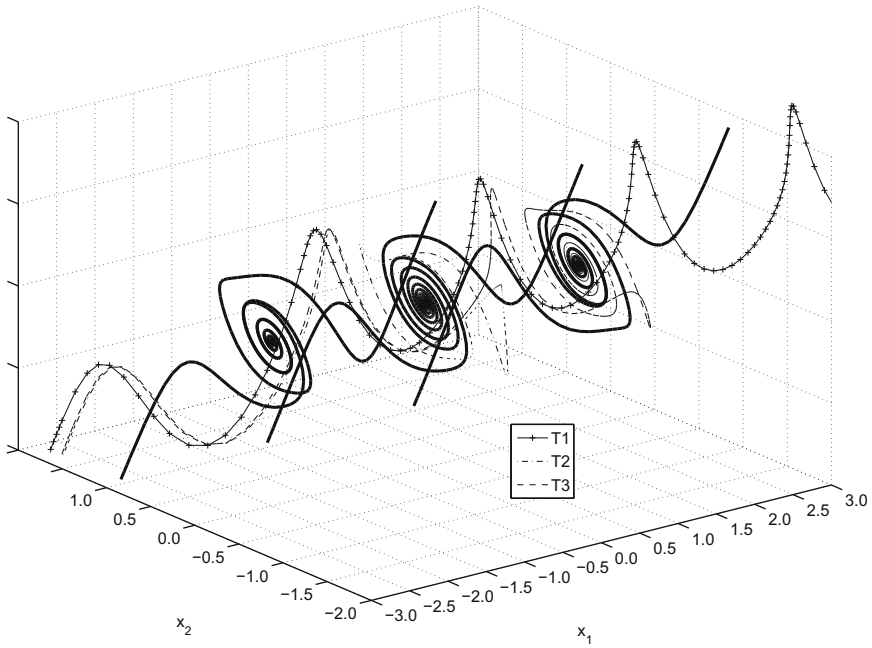

(a) 3D view.

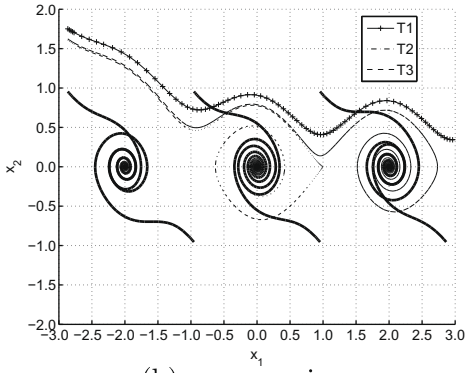

(b) $x_1 \times x_2$ view.

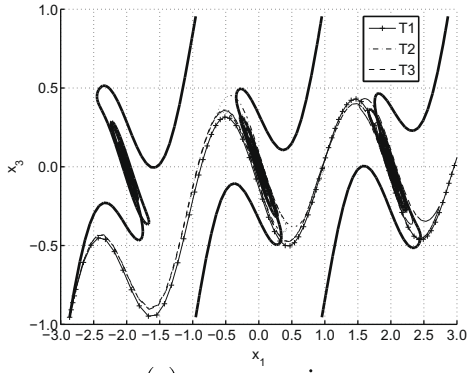

(c) $x_1 \times x_3$ view.

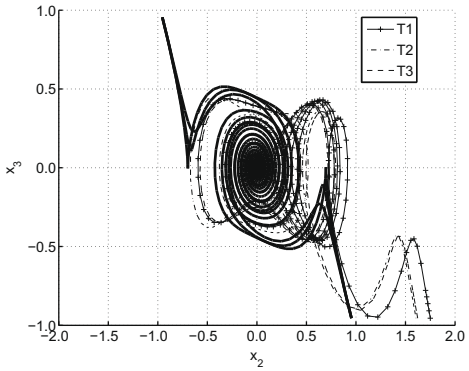

(d) $x_2 \times x_3$view.

Fig. 6. State space plot considering filter F_2, in units of π.

References

[1] Bregni S. Synchronization of digital networks. 1st ed. England: John Wiley & Sons; 2002.
[2] Lindsey WC, Ghazvinian F, Hagmann WC, Dessouky K. Network synchronization. Proc IEEE 1985;3:1445–67.
[3] Meyr H, Ascheid G. Synchronization in digital communications phase-frequency-locked loops, and amplitude control, vol. 1. England: John Wiley & Sons; 1990.
[4] Piqueira JRC, Monteiro LHA. All-pole phase-locked loops: calculating lock-in range by using Evan's root-locus. Int J Control 2006;79(7):822–9.
[5] Ferreira AA, Bueno AM, Piqueira JRC. Modeling and measuring double-frequency jitter in one-way master-slave networks. Commun Nonlinear Sci Numer Simul 2009;5(14):1854–60.
[6] Gardner FM. Phaselock techniques. 3rd ed. England: John Wiley & Sons; 2005.
[7] Piqueira JRC, Monteiro LHA. Considering second-harmonic terms in the operation of the phase detector for second order phase-locked loop. IEEE Trans Circuits Syst I 2003;50(6):805–9.
[8] Piqueira JRC, Takada EY, Monteiro LHA. Analyzing the effect of the phase-jitter in the operation of second order phase-locked loops. IEEE Trans Circuits Syst II 2005;52(6):331–5.
[9] Piqueira JRC, Caligares AZ. Double-frequency jitter in chain master-slave clock distribution networks: comparing topologies. J Commun Networks 2006;8(1):8–12.
[10] Piqueira JRC, Caligares AZ, Monteiro LHA. Double-frequency jitter figures in master-slave PLL networks. AEU – Int J Electron Commun 2007;61(10):678–83.
[11] Piqueira JRC, Castillo-Vargas SA, Monteiro LHA. Two-way master-slave double-chain networks: limitations imposed by linear master drift for second-order PLLs as slave nodes. IEEE Commun Lett 2005;9(9):829–31.
[12] Gardner FM. Charge-pump phase-lock loops. IEEE Trans Commun 1980;28(11):1849–58.
[13] Hedayat CD, Hachem A, Leduc Y, Benbassat G. Modeling and characterization of the 3*rd* order charge-pump PLL: a fully event-driven approach. Analog Integr Circ Signal Proc 1999;19:25–45.
[14] Hanuolu K, Brownlee M, Mayaram K, Moon Un-Ku. Analysis of charge-pump phase-locked loops. IEEE Trans Circ Syst I: Regular Papers 2004;51(9):1665–74.
[15] Piqueira JRC, Freschi MC. Models for master-slave clock distribution networks with third-order phase-locked loops. Math Probl Eng 2007. doi:10.1155/2007/18609. Article ID 18609.
[16] Monteiro LHA, Favaretto DN, Piqueira JRC. Bifurcation analysis for third-order phase-locked loops. IEEE Signal Proc Lett 2004;11(5):494–6.
[17] Piqueira JRC. Using bifurcations in the determination of lock-in ranges for third-order phase-locked loops. Commun Nonlinear Sci Numer Simul 2009;5(14):2328–35.
[18] Piqueira JRC, Marmo CN, Monteiro LHA. Using central manifold theorem in the analysis of master-slave synchronization networks. J Commun Networks 2004;6(3):197–202.
[19] Best RE. Phase-locked loops: design, simulation and applications. New York: McGraw-Hill; 2003.
[20] Kailath T. Linear systems. Englewood Cliffs, NJ: Prentice-Hall; 1980.
[21] Guckenheimer J, Holmes P. Nonlinear oscillations, dynamical systems, and bifurcation of vector fields. 2nd ed. Berlin: Springer; 1983.
[22] Ogata K. Modern control engineering. Prentice-Hall; 2002.
[23] Lynch S. Dynamical systems with applications using MATLAB. Boston: Birkhauser; 2004.
[24] Carareto R, Orsatti FM, Piqueira JRC. Reachability of the synchronous state in a mutually connected PLL network. AEU – Int J Electron Commun. doi:10.1016/j.aeue.2008.07.008.
[25] Wiggins S. Introduction to applied nonlinear dynamical systems and chaos. Berlin: Springer; 1990.
[26] Isidori A. Nonlinear control systems. Berlin: Springer; 1995.